BMC Biology

RESEARCH ARTICLE

Open Access

TRPM4 regulates hilar mossy cell loss in temporal lobe epilepsy

Laura Mundrucz[1†], Angéla Kecskés[2,3†], Nóra Henn-Mike[1,3], Péter Kóbor[1], Péter Buzás[1], Rudi Vennekens[4] and Miklós Kecskés[1*]

Abstract

Background Mossy cells comprise a large fraction of excitatory neurons in the hippocampal dentate gyrus, and their loss is one of the major hallmarks of temporal lobe epilepsy (TLE). The vulnerability of mossy cells in TLE is well known in animal models as well as in patients; however, the mechanisms leading to cellular death is unclear.

Results Transient receptor potential melastatin 4 (TRPM4) is a Ca^{2+}-activated non-selective cation channel regulating diverse physiological functions of excitable cells. Here, we identified that TRPM4 is present in hilar mossy cells and regulates their intrinsic electrophysiological properties including spontaneous activity and action potential dynamics. Furthermore, we showed that TRPM4 contributes to mossy cells death following status epilepticus and therefore modulates seizure susceptibility and epilepsy-related memory deficits.

Conclusions Our results provide evidence for the role of TRPM4 in MC excitability both in physiological and pathological conditions.

Keywords TRPM4, Mossy cell, Epilepsy, Ion channel

Background

Temporal lobe epilepsy (TLE) is a life-threating neurological syndrome characterized by recurrent seizures and an increased risk for a wide range of cognitive disorders [1]. Anti-epileptic drugs are ineffective in about 30% of patients demonstrating the urgent need to better understand the pathological mechanisms underlying epileptic seizures [2].

Partial loss of the hilar mossy cells (MC) of the hippocampus is one of the main hallmarks of TLE [3]. MCs are key excitatory neurons of the hippocampus innervating the granule cells (GC) of the dentate gyrus as well as GABAergic interneurons of the hilus [4]. They receive their major excitatory input from GCs via giant synaptic buttons onto large spine complexes along their proximal dendrites [5]. This results in a complex feedback microcircuit: MCs can directly excite GCs as well as indirectly inhibit them via GABAergic interneurons [6]. The opposing effects of MC activation led to debates whether the net effect of MC activation to GCs is inhibitory or excitatory in physiological conditions as well as in epilepsy [7]. Recently, it has been suggested that MC activation can result in a net inhibitory effect on the hippocampus indicating that MC loss in TLE can be an important mechanism leading to recurrent seizures [8]. However, another recent study found that selective MC inhibition

†Laura Mundrucz and Angéla Kecskés share first authorship.

*Correspondence:
Miklós Kecskés
kecskes.miklos@pte.hu
[1] Institute of Physiology, Medical School, University of Pécs, Pécs 7624, Hungary
[2] Department of Pharmacology and Pharmacotherapy, Medical School, University of Pécs, Pécs 7624, Hungary
[3] Szentagothai Research Centre, Centre for Neuroscience, University of Pécs, Pécs 7624, Hungary
[4] Laboratory of Ion Channel Research, Biomedical Sciences Group, Department of Cellular and Molecular Medicine, VIB-KU Leuven Center for Brain & Disease Research, KU Leuven, Louvain 3000, Belgium

decreases status epilepticus severity [9]. Despite the often controversial results about the exact role of MCs in hippocampal excitability, their extreme vulnerability in TLE has been well-established in rodent models as well as in human patients [10].

Indeed, one of the most exciting questions about MCs is the reason for their vulnerability in TLE. A possible mechanism suggests that an initial insult resulting in over-excitation of the local circuits presynaptic to MCs increases intracellular calcium and sodium up to a toxic level [11]. Another potential explanation is related to the intrinsic electrophysiological properties of the MCs: these cells are characterized by a low threshold for action potential, weak repolarization with practically no after hyperpolarization (AHP) and broad action potential (AP) [12]. Therefore, a strong and long-lasting excitatory input can easily lead to over excitation, depolarization block, and cellular death [3]. Clearly, the unique ion channel expression profile of the MCs leading to the above detailed electrophysiological properties might explain both hypotheses, yet the exact mechanism remains uncertain.

It has been shown already that calcium activated depolarizing currents are responsible for action potential duration and repolarization dynamics in other excitable cell types [13, 14]. The ion channels carrying this particular current belong to the superfamily of transient receptor potential (TRP) ion channels, called transient receptor potential melastatin 4 (TRPM4) and transient receptor potential melastatin 5 (TRPM5) [15].

In neurons, TRPM4-dependent membrane depolarization can support bursts of action potentials as it was shown in pre-Botzinger complex neurons [16, 17]. Furthermore, it can also mediate axonal and neuronal degeneration and cellular death in the animal model of experimental autoimmune encephalomyelitis and multiple sclerosis [18]. In line with the above-mentioned properties, we hypothesized that TRPM4 might play a role in the physiological function of MCs, as well as in the neuronal loss seen in TLE. However, until now, there was no information available about the expression and function of TRPM4 on MCs of the dentate gyrus.

Here, with a battery of histological, electrophysiological, and behavioral experiments we demonstrate for the first time that (i) *Trpm4* is present in hilar MC, (ii) plays a role in their intrinsic electrophysiological properties, (iii) contributes to MC death following status epilepticus (SE) and therefore (iv) modulates seizure susceptibility, and (v) epilepsy-related memory deficits in the chronic phase of experimental TLE. Altogether, our results shed light on a previously unrecognized role of TRPM4 in neuronal excitability both in healthy and overexcited hippocampus.

Results

Trpm4 is expressed in hilar MCs

To examine whether *Trpm4* is expressed in hilar MCs, we used RNAscope in situ hybridization for its high sensitivity to detect even low level of expression. Unfortunately, immune-histochemical detection of TRPM4 protein is often controversial in the literature [19]. Using RNAscope in situ hybridization within the hippocampal formation, we found abundant *Trpm4* mRNA expression primarily in the hilar region (Fig. 1A–C). No expression was detectable in granule cells of the dentate gyrus. The high level of RNAscope signal in the hilus was consistent with the expression pattern found at the Allen Brain Atlas. To clarify which cell type in the hilus is expressing

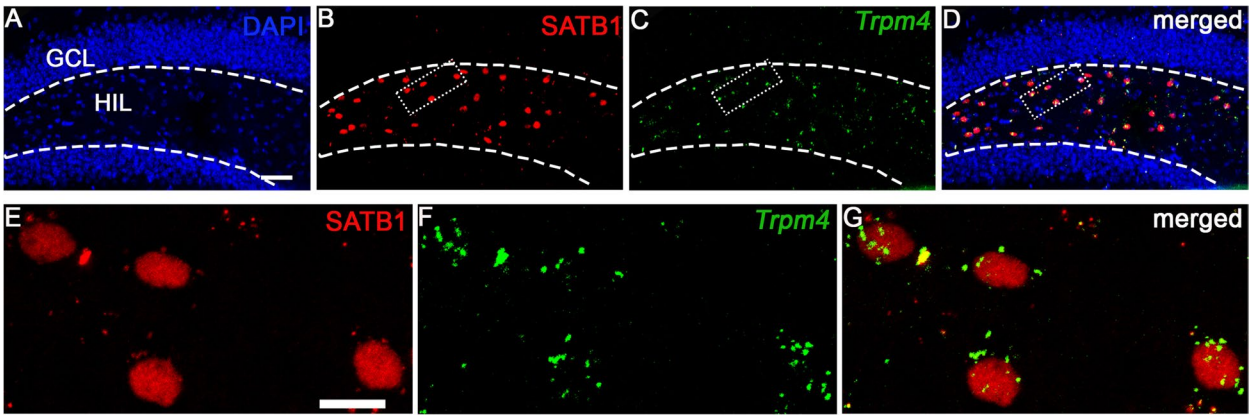

Fig. 1 *Trpm4* is expressed in SATB1-positive hilar mossy cells. Representative 10x (**A**–**D**) and 60x (**E**–**G**) confocal images of immunofluorescence staining for SATB1 (red) and RNAscope labeling of *Trpm4* (green) from 3 independent experiments. Cell nuclei are stained with DAPI. Note that SATB1 stains exclusively the nucleus of neurons; therefore, *Trpm4* signal in the close proximity of SATB1 is likely in the cytoplasm of MCs. Note that *Trpm4* is specifically expressed in MCs, but it is lacking from GCs. Scale bar 50 µm (upper row) and 5 µm (lower row)

Trpm4, we performed combined RNAscope and immunostaining using a novel molecular marker for MCs, special AT-rich sequence-binding protein 1 (SATB1). SATB1 is a transcriptional factor used as a neuronal marker in different brain areas [20] including the hilus [21]; however, its expression in MCs has never been directly shown. Double staining experiments using the MC marker GluR2/3 [22] showed that 94.4 ± 1.2% of SATB1 positive cells were also GluR2/3 positive and 97.5 ± 1% of GluR2/3 positive cells were also SATB1 positive in the hilar region (Fig. S1). Since SATB1 stained exclusively MCs in the hippocampus contrary to GluR2/3, we therefore used this marker in our further experiments. Our combined *Trpm4* RNAscope and SATB1 immunostaining study clearly showed that the majority of SATB1 positive hilar MCs also express *Trpm4* (Fig. 1A–G).

TRPM4 contributes to intrinsic electrophysiological properties of hilar MCs

In order to test whether TRPM4 is functionally active on hilar MCs, we performed patch clamp recordings in acute brain slices containing the hippocampal formation. Randomly selected biocytin filled neurons were immunostained with the novel MC marker SATB1 (Fig. S2) for post hoc identification. Since there is no available selective and potent pharmacological blocker of TRPM4—the most often used TRPM4 blocker, 9-phenantrol is only partially selective [23, 24]—we used *Trpm4*$^{-/-}$ mice to explore the role of the channel in MCs. Considering the timing of the increase in intracellular Ca^{2+} concentration relative to the neuronal AP [25], we assumed that a calcium activated cationic current might affect the repolarization phase of the AP. Indeed, when we compared AP parameters between WT and *Trpm4*$^{-/-}$ MCs, we found significantly greater after hyperpolarization (WT = −2.5 ± 0.2 mV, *Trpm4*$^{-/-}$ = −4.3 ± 0.6 mV, $p = 0.0049$, two sample *T*-test) in neurons lacking TRPM4 indicating the absence of a depolarizing current during the late phase of the AP (Fig. 2A). It has been shown previously that MCs are intrinsically active both in vivo and in vitro [4, 22]; therefore, we explored whether this intrinsic activity is modulated by the action of TRPM4. Current clamp recordings revealed that the amplitude of the spontaneous EPSPs (WT = 5.0 ± 0.4 mV, *Trpm4*$^{-/-}$ = 4.0 ± 0.2 mV, $p = 0.03$, two sample *T*-test) and the frequency of the spontaneous APs (WT = 1.3 ± 0.2 Hz, *Trpm4*$^{-/-}$ = 0.5 ± 0.1 Hz, $p = 0.0019$, two sample *T*-test) were both significantly lower in MCs lacking TRPM4 (Fig. 2B, C). Finally, we challenged the cells with high concentration of glutamate (1 mM) mimicking excitotoxicity. Glutamate application increased the spontaneous AP frequency both in WT and *Trpm4*$^{-/-}$ MCs; however, WT neurons reached depolarization block (AP amplitude decreased with more than 50%) more frequently than *Trpm4*$^{-/-}$ cells (WT = 6 out of 7 cells, *Trpm4*$^{-/-}$ 1 out of 6 cells $p = 0.029$, Fischer's exact test, Fig. 2D). To further support our electrophysiological findings, we applied 9-phenanthrol (30 µM) on WT MCs to block TRPM4 current. Application of the non-selective TRPM4 blocker significantly decreased spontaneous firing frequency of WT MCs (ACSF = 1.4 ± 0.2 Hz, 9-phenanthrol = 0.44 ± 0.1 Hz, wash = 1.3 ± 0.2 Hz, $p = 0.006$, one-way ANOVA with Tukey's post hoc test, Fig. 2E). Other basic electrophysiological parameters including resting membrane potential (WT = −63 ± 5 mV, *Trpm4*$^{-/-}$ = −63 ± 6 mV) and input resistance (WT = 137 ± 11 MΩ, *Trpm4*$^{-/-}$ = 131 ± 10 MΩ) were not significantly different between genotypes.

Trpm4$^{-/-}$ MCs are less vulnerable in experimental TLE compared to WT MCs

To examine MC vulnerability in experimental TLE, we used the intrahippocampal kainic acid model (IHKA) [26]. KA was injected into the left dorsal hippocampus of WT and *Trpm4*$^{-/-}$ mice. In our pilot experiments, the concentration of KA (20 mM, 100 nL) often used in experimental model of TLE led to the practically complete elimination of MCs ipsilateral to the injection site (unpublished observation). Therefore, we decided to use a lower concentration (5 mM, 100 nL) to partially eliminate MCs and evaluate the effect of SE cell-specifically. This concentration of KA led to behavioral seizures in most of the injected mice. The seizures were scored based on the Racine's scale, and SE was considered successful if grade 3 or higher seizures were observed. Using this method, we were assured that all mice used in our study experienced severe seizures in the first 2 h after IHKA. To determine whether the lack of TRPM4 affected MC loss after SE, WT and *Trpm4*$^{-/-}$ mice were sacrificed 14 days after KA injection. Brains were sectioned in the coronal plane and immunostained with SATB1 to evaluate MC loss in the hilus both ipsilateral and contralateral to the KA injection (Fig. 3A–C). From each mouse, 10 sections were collected through the anterior–posterior length of the hippocampus and the average number of MCs per section was determined. These experiments revealed that SE resulted in significantly lower cellular survival rate in WT mice compared to *Trpm4*$^{-/-}$ ipsilateral to KA injection (Fig. 3D) ($WT_{epileptic} = 19 \pm 16\%$, $Trpm4^{-/-}{}_{epileptic} = 54 \pm 10\%$, $p = 0.00025$, one-way ANOVA with Tukey's post hoc test). Same tendency was present in the contralateral side although the difference was not significant (Fig. 3E).

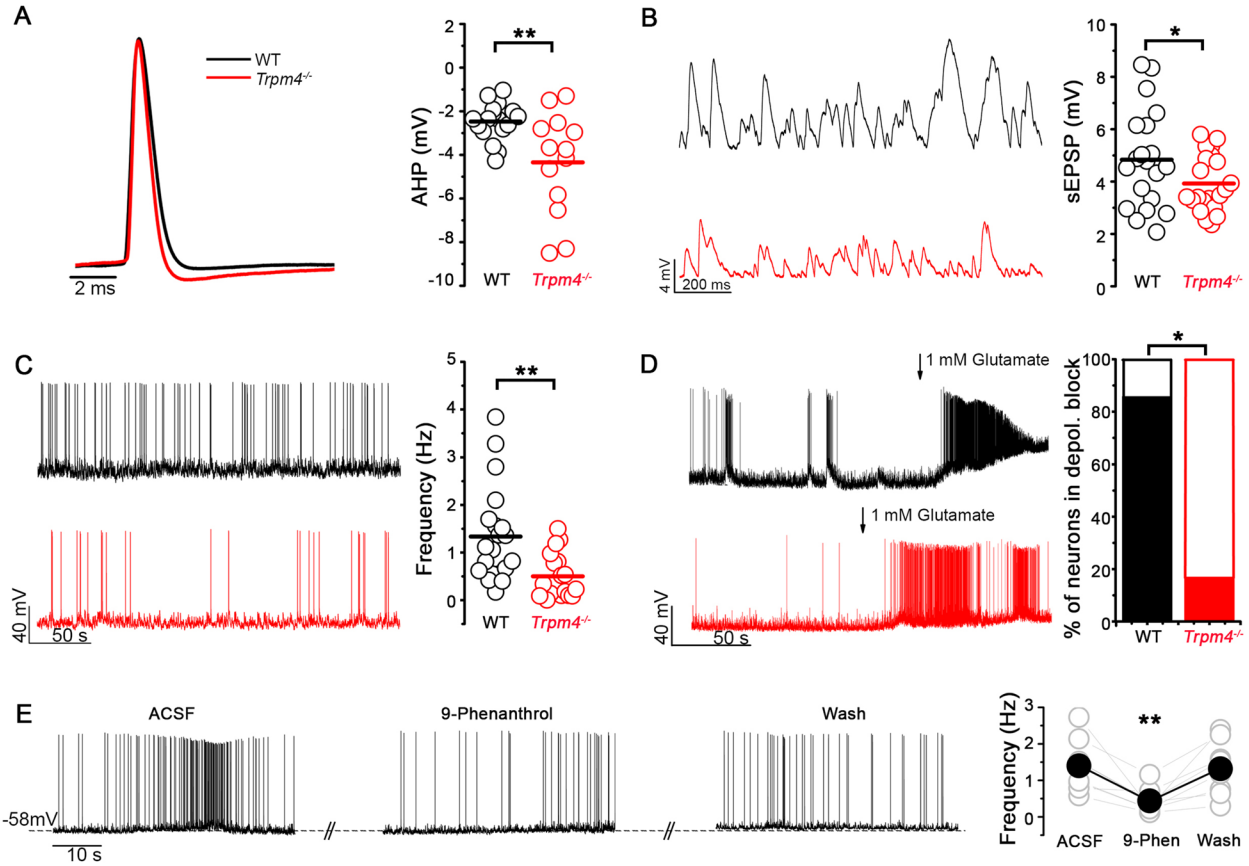

Fig. 2 TRPM4 contributes to intrinsic electrophysiological properties of MCs. **A** Left, overlay of APs from WT (black) and *Trpm4*$^{-/-}$ (red) MCs induced by current injection. Amplitudes of the representative APs are normalized to each other for better visibility. Right, statistics of AHPs from WT and *Trpm4*$^{-/-}$ MCs. $n = 17$ for WT and 13 for *Trpm4*$^{-/-}$. **B** Left, representative traces of EPSPs from WT and *Trpm4*$^{-/-}$ MCs. Right, statistics of sEPSP from WT and *Trpm4*$^{-/-}$ MCs. $n = 19$ for WT and 21 for *Trpm4*$^{-/-}$. **C** Left, representative spontaneous APs from WT and *Trpm4*$^{-/-}$ MCs. Right, statistics of AP frequency from WT and *Trpm4*$^{-/-}$ MCs. $n = 20$ for WT and 19 for *Trpm4*$^{-/-}$. **D** Left, representative current clamp recordings from WT and *Trpm4*$^{-/-}$ MCs upon 1 mM glutamate application. Right, statistics showing the percentage of neurons in depolarization block. $n = 7$ for WT and 6 for *Trpm4*$^{-/-}$. **E** Left, representative spontaneous APs from WT MCs in ctrl condition, upon application of 9-phenanthrol and after wash out of the drug. Right, statistics showing AP frequency from WT MCs during the three mentioned conditions $n = 9$. $^{*}p < 0.05$, $^{**}p < 0.01$

Trpm4$^{-/-}$ mice display decreased seizure susceptibility compared to WT mice

Next, we investigated whether the better survival of MCs in *Trpm4*$^{-/-}$ mice after SE also resulted in less frequent and severe spontaneous seizures during the chronic phase of the IHKA model. First, we were interested in whether we can detect interictal epileptic discharges (IED) preceding epileptic seizures in IHKA model [27]. WT and *Trpm4*$^{-/-}$ mice underwent videoEEG recording 2 weeks after KA injection. Each mouse was monitored for 1 h/day at the same time on 3 consecutive days (Fig. 4A, B). These experiments clearly showed a significantly increased number of IEDs in WT mice compared to *Trpm4*$^{-/-}$ mice (Fig. 4D) (WT = 66 ± 36 IED/h, *Trpm4*$^{-/-}$ = 24 ± 24 IED/h, $p = 0.017$, Mann–Whitney test) indicating an increased hippocampal excitability. To examine the spontaneously occurring seizures we performed 24-h videoEEG recordings 2–3 weeks after KA injection. The relatively low KA concentration used in our experimental protocol resulted in occasional seizures only (1 seizure from 3 WT mice during 24 h). Therefore, we decided to synchronize seizures with the injection of sub-threshold dose of KA intraperitoneally (i.p.). The sub-threshold dose of KA (5 mg/kg BW) resulted in no detectable seizures in healthy WT mice in line with previous observations [28]; however, it induced both electrographic and behavioral seizures in IHKA mice (Fig. 4C). Both the number of seizures (WT = 7.3 ± 5 seizures/2 h, *Trpm4*$^{-/-}$ = 1.5 ± 2 seizures/2 h $p = 0{,}032$, Mann–Whitney test) and the total seizure duration (WT = 1186 ± 1296 s/2 h, *Trpm4*$^{-/-}$ = 337 ± 730 s/2 h

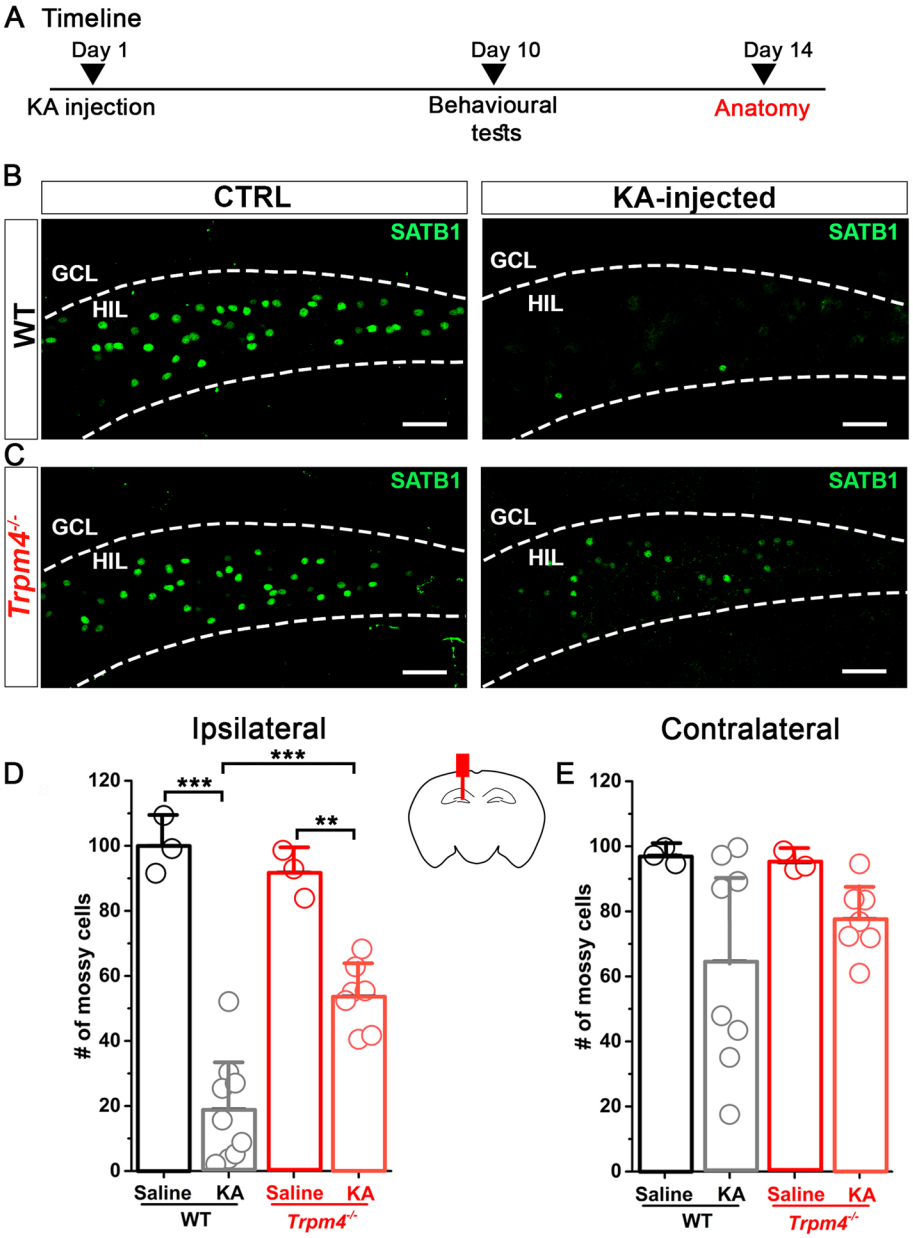

Fig. 3 *Trpm4*$^{-/-}$ MCs are more protected after KA injection compared to WT MCs. **A** Timeline of the experiments. Mice underwent KA or saline (ctrl) injection. Ten days later, behavioral tests were performed to assess spatial and contextual memory (detailed in: Fig. 5). At day 14, mice were sacrificed for histological studies. Representative 10 × confocal images of SATB1immunopositive neurons in the hilus from WT (**B**) and *Trpm4*$^{-/-}$ (**C**) ctrl (left side) and KA (right side) injected mice. Statistics showing the number of MCs in WT and *Trpm4*$^{-/-}$ mice ipsilateral (**D**) and contralateral (**E**) to the site of the injection. $n = 3$ for $WT_{ctrl,}$ 9 for $WT_{KA,}$ 3 for $Trpm4^{-/-}{}_{ctrl,}$ and 7 for $Trpm4^{-/-}{}_{KA.}$ Cell numbers are normalized to the saline injected WT group. Scale bar 50 µm. Data are presented as mean ± SD. *$p < 0.05$, **$p < 0.01$; ***$p < 0.001$

$p = 0{,}088$, Mann–Whitney test) were significantly lower in *Trpm4*$^{-/-}$ mice in the first 2 h following the i.p. KA injection (Fig. 4E, F). Interestingly, no difference was visible between the genotypes concerning the individual spikes (Fig. 4G). Furthermore, theta, alpha, beta, and gamma power spectra were compared between epileptic WT and *Trpm4*$^{-/-}$ mice during free exploration 2 weeks after IHKA, but no significant changes were detected (Fig. S3).

TRPM4 deletion rescues memory impairment in chronically epileptic mice

To investigate the role of TRPM4 in memory impairment often seen in chronically epileptic mice [29], we performed

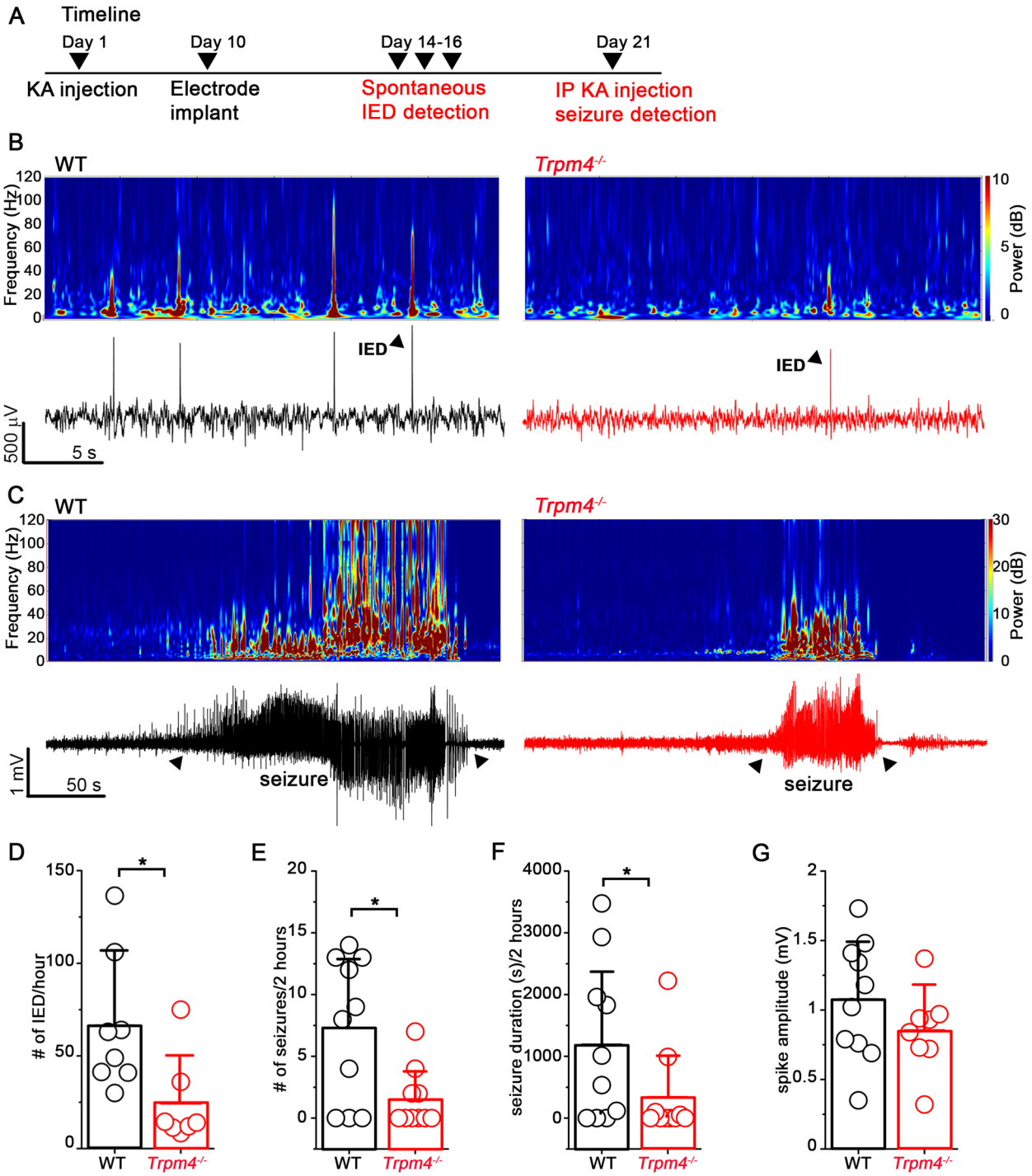

Fig. 4 Increased seizure susceptibility in KA injected WT mice compared to *Trpm4*$^{-/-}$. **A** Timeline of the experiments. Mice underwent KA or saline (ctrl) injection. Ten days later EEG electrodes were implanted. Fourteen days later, mice underwent spontaneous IED detection; 21 days later seizures were induced with i.p. KA injection and detected with videoEEG. **B** Representative EEG recordings (lower panel) and corresponding spectrograms (upper panel) 14 days after KA injection in WT (black) and *Trpm4*$^{-/-}$ (red) mice. Triangles indicate individual IED events. **C** Representative EEG recordings (lower panel) and corresponding spectrograms (upper panel) 21 days after KA injection in WT (black) and *Trpm4*$^{-/-}$ (red) mice after KA injection. Triangles indicate seizures. **D** Statistics showing the number of spontaneous IED/h 14 days after IHKA. $n = 8$ for WT and 7 for *Trpm4*$^{-/-}$. Statistics showing the **E** number of seizures, **F** seizure duration, and **G** spike amplitude in 2 h after i.p. KA injection. $n = 10$ for WT and 10 for *Trpm4*$^{-/-}$. Data are presented as mean ± SD. *$p < 0.05$

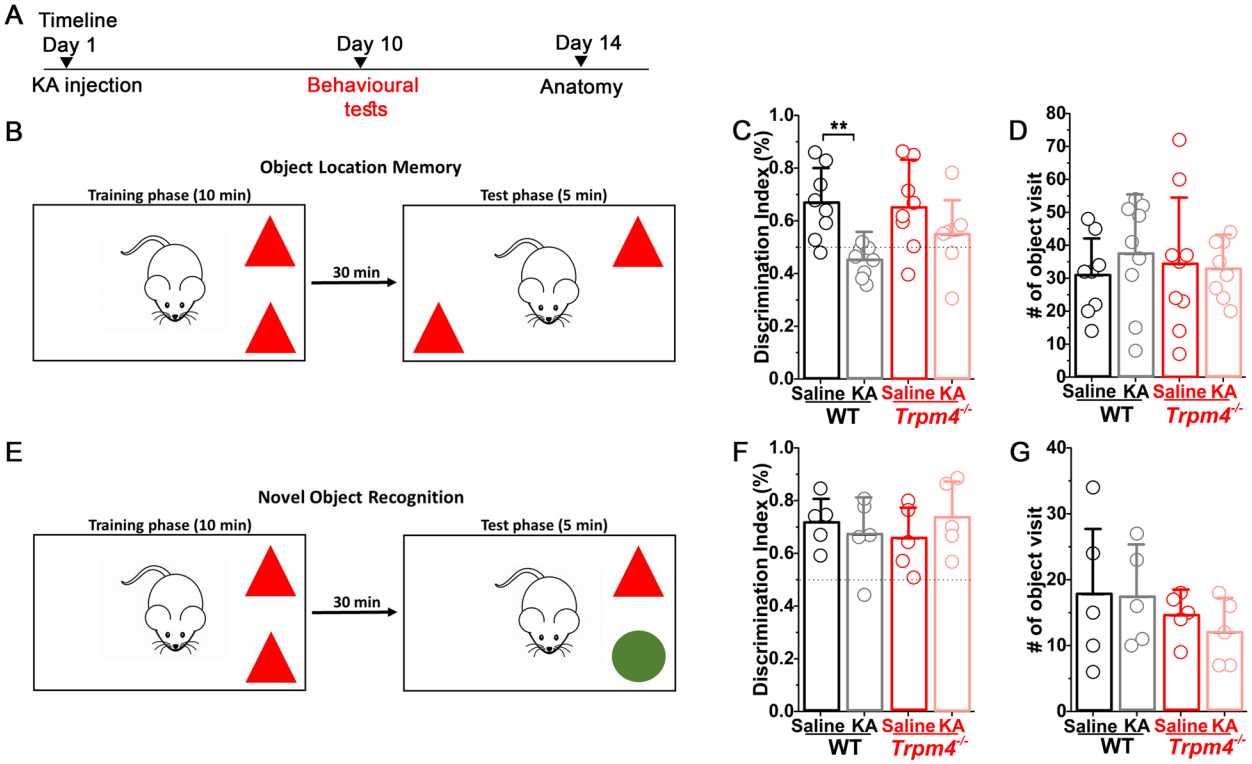

Fig. 5 Epileptic WT but not $Trpm4^{-/-}$ mice have impaired spatial memory. **A** Timeline of the experiments. Mice underwent KA or saline (ctrl) injection. Ten days later, behavioral tests were performed to assess spatial and contextual memory. **B** OLM test schematic and timeline. Statistics showing discrimination index (**C**) and number of object visit (**D**) in WT and $Trpm4^{-/-}$ mice. $n = 8$ for $WT_{ctrl,}$ 9 for $WT_{KA,}$ 9 for $Trpm4^{-/-}{}_{ctrl,}$ and 8 for $Trpm4^{-/-}{}_{KA.}$ **E** OLM test schematic and timeline. Statistics showing discrimination index (**F**) and number of object visit (**G**) in WT and $Trpm4^{-/-}$ mice. $n = 5$ for $WT_{ctrl,}$ 5 for $WT_{KA,}$ 5 for $Trpm4^{-/-}{}_{ctrl,}$ and 5 for $Trpm4^{-/-}{}_{KA.}$ Data are presented as mean ± SD. $^{*}p < 0.05$, $^{**}p < 0.01$, $^{***}p < 0.001$

object location memory (OLM) and novel object recognition (NOR) tests on control (saline injected) and epileptic mice on both genotypes (Fig. 5A). Chronically epileptic WT mice had significant deficits in OLM test and were unable to distinguish the object in novel position from the unmoved object (Fig. 5B, C). Interestingly, in epileptic $Trpm4^{-/-}$ mice, this significant deficit was not present as it is reflected in the discrimination index ($WT_{saline} = 0.66 \pm 0.13\%$, $WT_{epileptic} = 0.45 \pm 0.05\%$, $Trpm4^{-/-}{}_{saline} = 0.65 \pm 0.16\%$, $Trpm4^{-/-}{}_{epileptic} = 0.54 \pm 0.13\%$, $p = WT_{saline}$ vs $WT_{epileptic} = 0.002$, $Trpm4^{-/-}{}_{saline}$ vs $Trpm4^{-/-}{}_{epileptic} = 0.11$, Kruskal–Wallis test). On the contrary, NOR test showed no deficit in chronically epileptic mice neither in WT nor in $Trpm4^{-/-}$ mice (Fig. 5E, F) indicating that this type of contextual memory is not effected in our IHKA epilepsy model. Of note, these observations were not because of altered mobility between groups since object visits were not significantly different among them (Fig. 5D, G).

Conclusions

In this study, we report that TRPM4 plays a pivotal role in MC loss during excitotoxic insults leading to SE. At the cellular level, we showed for the first time that *Trpm4* is present in hilar MCs and as a Ca^{2+} -activated cationic current regulates the spontaneous activity of MCs as well as the repolarization of their AP in physiological conditions. After IHKA, mice lacking TRPM4 showed reduced MC loss and seizure susceptibility during the chronic phase of the model. Our finding that $Trpm4^{-/-}$ mice show better performance in spatial memory tests after IHKA further supports its role in MC vulnerability during seizures. In summary, our results provide evidence for the role of TRPM4 in MC excitability both in physiological and pathological conditions.

Expression pattern of TRPM4 in the brain is controversial because of the lack of selective antibodies. Several studies suggested the role of TRPM4 in neuronal function on different brain regions including the hippocampus [19, 30, 31], the prefrontal cortex [32], and the pre-Bötzinger [33] complex; however, most of these publications used pharmacological tools with questionable selectivity [24] to investigate TRPM4 function. Recently, two studies proved the expression of *Trpm4* in brainstem pacemaker neurons using the ultrasensitive RNAscope in situ hybridization technique [34, 35]. Our findings extend these results. To our best knowledge, this

is the first evidence that the Ca^{2+} activated cation channel *Trpm4* transcripts are present in hilar MCs. Furthermore, during these histological studies we introduced SATB1 as a novel molecular marker with exclusive selectivity towards MCs within the hippocampus.

What is the physiological role of TRPM4 in MCs? It has been shown previously that TRPM4-dependent membrane depolarization can contribute to the time course of the AP, as it was shown in cardiac myocytes, or it can support bursts of action potentials in neurons [13, 14, 17]. Furthermore, it can also mediate axonal and neuronal degeneration and glutamate mediated excitotoxicity in the animal model of experimental autoimmune encephalomyelitis [18]. In accordance, in our experiments, we found an increased after-hyperpolarization in *Trpm4*$^{-/-}$ MCs possibly indicating the lack of a Ca^{2+} activated depolarizing current at the late phase of the AP. Furthermore, MCs lacking TRPM4 displayed significantly decreased spontaneous AP firing frequency as well as decreased EPSP amplitude. Based on these observations, we hypothesize that during excitatory postsynaptic events the increased calcium level activates TRPM4 and therefore amplifies EPSPs arriving onto MCs and increases excitability of these cells. During an AP, the depolarizing current via TRPM4 will counterbalance the end of the repolarization phase, which results in weak or no AHP commonly observed in MCs [3]. Of note, this would imply that TRPM4 is expressed both in the synapse and on the soma of MCs. Therefore, it would be of great interest to conduct sub-cellular localization studies to precisely map TRPM4 expression. Moreover, one can speculate that the amplifier function of TRPM4 is an effective mechanism to enhance the inputs from the otherwise sparsely active GCs in physiological conditions, while during pro-epileptic insults it can worsen the excitotoxicity caused by the hyperexcited circuit. Indeed, challenging these cells with glutamate *Trpm4*$^{-/-}$ MCs were less frequently entered into depolarization block compared to WT MCs. Interestingly, we also detected moderate expression of *Trpm4* in CA3 neurons (data not shown). Further experiments are needed to clarify whether this also affects MC excitability via back-projecting axons. Indeed, MCs receive their major synaptic inputs from GCs. Based on our RNAscope experiments, *Trpm4* transcripts are absent in GCs; therefore, it is unlikely that the global deletion of TRPM4 would indirectly effect MCs via presynaptic GCs. However, given the important role of back-projecting CA3 axons to MCs, we cannot exclude the possibility that deletion of TRPM4 from CA3 neurons as well might indirectly affect MCs and therefore influences our findings.

Direct injection of KA into the hippocampal formation (IHKA) results in SE, widespread cellular death among hilar MCs, and often the appearance of spontaneous seizures [26]. In principle, it is possible to record EEG immediately after IHKA; however, this approach requires longer anesthesia because of the electrode implantation that influences seizures [36]. Therefore, to test whether IHKA induced SE, we used the Racine's scale scores. This method is less sensitive as EEG recordings since the electrographic seizures without motor manifestation are undetectable; however, if grade 3 or higher score is identified, one can be sure that those mice underwent severe seizures, and we used only these mice in subsequent experiments.

MCs are in a key position to regulate both the onset of epileptogenesis and the recurrent seizures during the chronic phase of epilepsy [5, 6]. Our observation that MCs lacking TRPM4 are more protected during SE is probably the result of their reduced spontaneous activity, which is in line with previous observations that inhibiting MC during SE decreases MC and CA3 neuronal loss [9]. It is common view that the initial SE in TLE is followed by a seizure free period that precedes the development of spontaneous seizures and IED in between seizures [37]. In our experiments, the reduced MC loss in *Trpm4*$^{-/-}$ mice resulted in less frequent IEDs indicating that the overall excitability of the hippocampal circuit is reduced in these mice. Interestingly, despite the occurrence of IEDs in both genotypes after IHKA, spontaneously occurring seizures were rare. The reason for that most likely lies on the relatively low concentration of KA we used in our IHKA experiments. Nevertheless, this concentration range allowed us to more specifically investigate MC vulnerability between the two genotypes since the classically used higher dose practically killed more than 90% of MCs in both genotypes, not surprisingly since MCs are one of the most vulnerable cell types during epileptic insults [5]. Although spontaneous seizures were rare in our experimental protocol, the seizure susceptibility clearly increased in IHKA mice. The subthreshold dose of i.p. KA injection did not result in seizures in naïve mice while it induced both electrographic and behavioral seizures in previously KA injected mice in both genotypes. It has to be noted however that these are evoked seizures and not spontaneously occurring ones therefore our model is not mimicking perfectly chronic phase of epilepsy. However, our findings that the induced seizures were less frequent and shorter in duration in case of *Trpm4*$^{-/-}$ mice further support the protective role of TRPM4 elimination from MCs in epileptic conditions. Although in our experimental settings it is difficult to collect EEG data during the SE induction, the most likely explanation for the above detailed results is that SE is less severe in *Trpm4*$^{-/-}$ mice. Further experiments are needed to directly test this possibility.

Finally, we found that the reduced loss of MCs in *Trpm4*$^{-/-}$ mice during IHKA results in better performance in spatial memory test. Interestingly, behavioral paradigms testing contextual novelty instead of spatial novelty has not changed in any of the genotypes during epilepsy further supporting the recent findings that MCs have an important role in spatial memory encoding [22, 38].

Taken together, we report here that *Trpm4* is expressed in hilar MCs and regulates their AP waveform and spontaneous activity in physiological conditions. Furthermore, during SE, TRPM4 contributes to MC loss and increase seizure susceptibility. Our results are especially important in the light of recent findings identifying TRPM4 as a promising drug target in cardiac arrhythmias [39] especially because it has been shown that this type of arrhythmia is often associated with seizures [40]. Thus, TRPM4 might be a common regulator of Ca^{2+} dependent excitability both in cardiac myocytes and neurons. Better understanding how TRPM4 regulates MC excitability may lead to novel strategies in seizure management and could highlight its clinical importance.

Methods

Experimental animals

Experiments were performed on 3- to 6-month-old male C57BL/6N mice and age matched *Trpm4*$^{-/-}$ mice. The *Trpm4*$^{-/-}$ mice line was breed in homozygous form, and after every 4th generation, they were backcrossed into C57BL/6N background. For the genotyping, we used the following primers: WT and KO reverse 5′-gtt tga tgt ctc ctt cag tcg-3′; KO forward: 5′-gag ttc ctg tcc tcc taa agg-3′; WT forward: 5′-acc tac agg aaa cct cgg gg-3′. Mice were housed with a 12-h light/12-h dark cycle and allowed water and standard food ad libitum. All animal experiments were performed according to the European Community Council Directive and approved by the local ethics committee (Ethics Committee on Animal Research of Pécs, Hungary, BA02/2000–10/2020 and BA02/2000–56/2022).

Epilepsy induction and monitoring

Kainic acid (Sigma-Aldrich, *58002-62-3*) (100 nL, 5 mM in saline) was stereotaxically injected into the left hippocampus (2.0 mm posterior, 1.05 mm left, and 1.6 mm ventral to the bregma) using 1μL pipette (Hamilton, 25 g needle) under isoflurane anesthesia to induce status epilepticus (SE). We scored behavioral seizures based on the Racine's scale method only without EEG recordings, and SE induction was considered successful if grade 3 or higher seizures were observed. Mice showing no sign of SE were excluded from the subsequent experiments. Control mice were injected with saline in the same position. Seven to ten days after KA or saline injection, animals were stereotaxically implanted with two recording electrodes (tungsten, 0.05 mm, insulated, GoodFellow) (2.0 mm posterior, 1.05 mm left/right, and 1.6 mm ventral to the bregma) into both hippocampi, a reference (somatosensory cortex, 2.0 mm posterior, 2.3 mm left, and 0.5 mm ventral to the bregma) and a ground electrode (under the skin). Tungsten wires were soldered to a custom made 6 pin connector suitable to connect with the preamplifier. This connector was fixed into the scalp of the mouse using dental cement. After recovery from the implant procedure, mice underwent video EEG monitoring. During recordings, each mouse was individually placed into a 25 cm × 25 cm transparent cage. Same bedding, food, and water were supplied as during standard housing. For seizure detection, a preamplifier was inserted into the 6-pin connector via a multichannel commutator (Moflon Technology LTD, MC190). This system allowed the mice to freely move throughout the entire cage. EEG signal was acquired at 1 kHZ and band pass filtered at 1.6–2000 Hz (Supertech BioAmp, AD Instruments PowerLab, MultiChannel Systems, W2100). Data were acquired and analyzed using LabChart software (AD Instruments) and Brainstorm [41]. Synchronous video recordings were captured using a webcam (Alcor AWC1080). For spike analysis, we first determined standard deviation (SD) for each recording from a spike free "baseline" period using LabChart software. Spikes were considered as fast events (> 10 Hz) with amplitude higher than 3 SD of the given recording. Seizure was considered as train of spikes with at least a frequency of 0.5 Hz and a duration of 5 s. Seizures with no behavioral signs were considered as non-convulsive. Seizures with clear behavioral signs were considered as convulsive.

Slice preparation

In vitro patch clamp recordings were performed in acute horizontal brain slices taken from C57BL/6N and *Trpm4*$^{-/-}$ mice. Under deep isoflurane anesthesia, mice were decapitated, and horizontal slices (300 μm thick) were cut using a vibratome (Leica VS1200) in ice-cold external solution containing (in mM): 93 NMDG, 2.5 KCl, 25 Glucose, 20 Hepes, 1.2 $NaH2PO_4$, 10 $MgSO_4$, 0.5 $CaCl_2$, 30 $NaHCO_3$, 5 L-ascorbate, 3 Na-Pyruvate, 2 thiourea, bubbled with 95% O_2 and 5% CO_2. Slices were transferred to artificial cerebrospinal fluid (ACSF) containing (in mM) 2.5 KCl, 10 glucose, 126 NaCl, 1.25 NaH_2PO_4, 2 $MgCl_2$, 2 $CaCl_2$, 26 $NaHCO_3$ bubbled with 95% O_2 and 5% CO_2. After an incubation period of 10 min at 34 °C in the first solution, the slices were maintained at 20–22 °C in ACSF until use. After recordings,

the sections were immersed into fixative (4% paraformaldehyde in 0.1 M phosphate buffer) for overnight fixation.

In vitro electrophysiological recordings

Patch pipettes were pulled from borosilicate glass capillaries with filament (1.5 mm outer diameter and 1.1 mm inner diameter; Sutter Instruments, *BF150-110-7.5HP*) with a resistance of 2–3 MΩ. The pipette recording solution contained (in mM) 10 KCl, 130 K-gluconate, 1.8 NaCl, 0.2 EGTA, 10 HEPES, 2 Na-ATP, 0.2% Biocytin, pH 7.3 adjusted with KOH; 290–300 mOsm. Whole-cell recordings were made with Axopatch 700B amplifier (with Clampex 10.7 and Axoclamp1.1, Molecular Devices) using an upright microscope (Nikon Eclipse FN1, with × 40, 0.8 NA water immersion objective lens) equipped with differential interference contrast (DIC) optics. DIC images were captured with an Andor Zyla 5.5 sCMOS camera. All recordings were performed at 32 °C in ACSF bubbled with 95% O_2 and 5% CO_2. For AP parameter determination experiments, 1 µM CNQX (Sigma-Aldrich, *C-127*) was applied in the bath solution to eliminate EPSPs. Cells with < 20 MΩ access resistance (continuously monitored) were accepted for analysis. Signals were low-pass filtered at 5 kHz and digitized at 20 kHz (Digidata 1550B, Molecular Devices). In vitro data analysis was performed with the help of Clampfit 10.7 (Molecular Devices) and Origin 8.6 (OriginLab Corporation). When it is indicated 30 µM 9-phenanthrol (Sigma-Aldrich, *211281*) was applied into the bath solution.

Immunohistochemistry, RNAscope in situ hybridization, and confocal imaging

Two weeks after IHKA injection, animals were deeply anesthetized and transcardially perfused with ice-cold saline and then with 4% paraformaldehyde in 0.1 M PB (pH = 7.4). Brains and immersion fixed acute slices (patch clamp experiments) were cut into 60-µm-thick sections in the coronal plane with a vibratome (Leica, VS1000s). On selected sections, immunoreactivities were tested: SATB1 (mouse, 1:500, SantaCruz, *sc-376096*) and GluR 2/3 (rabbit, 1:500, Millipore, 07–598) were diluted in 0.1 M PB and incubated overnight at room temperature. For detection, fluorescent dye (Alexa488/Alexa594) conjugated donkey secondary antibodies (Jackson ImmunoResearch Labs, *715-545-150/715-585-150*) raised against the host species of primary antibodies were applied on the sections. To determine MC loss after SE, 10 sections (60 µm) per mouse (every third section) were collected starting from AP: − 1.4 mm to AP: − 3 mm from the bregma and all SATB1 positive cells in the hilus were counted. In certain sections, immunohistochemistry was combined with RNAscope in situ hybridization as described previously [42]. Confocal images were taken with a Nikon Eclipse Ti2-E confocal microscope with 10x and 20x objectives.

Object location and novel object memory test

Prior to the test, mice were habituated in the experimental room for 2 h. During training phase, the mice were allowed to freely explore the environment for 10 min with the presence of two identical objects (LEGO blocks). During test phase (30 min after training), the mice were placed again in the presence of two objects. For OLM test, the objects were the same, but one object was moved from the original location to a novel location. For NOR test, one object was replaced with a novel object (LEGO blocks with different shape and color), but the location remained the original. Testing trials were video-recorded and analyzed using the SolomonCoder software. Object exploration was quantified as the amount of time the mouse's nose spent touching the object. The exploration times were expressed as a discrimination index (D.I. = $(t_{novel}/t_{total}) \times 100$.

Statistics

Data are represented as mean ± SD. Normalities of samples were tested with Shapiro-Wilk test. Normally distributed samples were compared with Student's *T*-test; non-normally distributed data were compared with Mann–Whitney test. ANOVA test with Tukey post hoc test for normally distributed data and Kruskal-Wallis for non-normally distributed data were used for three or more group comparison.

Abbreviations

MC	Mossy cell
GC	Granule cell
IHKA	Intrahippocampal kainic acid injection
AHP	After hyperpolarization
SE	Status epilepticus
TLE	Temporal lobe epilepsy
SATB1	Special AT-rich sequence-binding protein 1
OLM	Object location memory
NOR	Novel object recognition
IED	Interictal epileptic discharge

Supplementary Information

The online version contains supplementary material available at https://doi.org/10.1186/s12915-023-01604-3.

Additional file 1. SATB1 and Glur2/3 are colocalized in the hilus. Representative 10xand 60xconfocal images of double immunofluorescence staining for SATB1and GLuR2/3.Left, percentage of SATB1 positive neurons that express GLuR2/3. Right, percentage of GLuR2/3 positive neurons that express SATB1. n = 211 neurons from 2 mice. Scale bar 100 µmand 5 µm.

Additional file 2. Patched neurons in the hilus are SATB1 positive. Representative confocal images of biocytinfilled WTand Trpm4−/−MCs counterstained with SATB1. Note that the biocytin filled cells are also

SATB1 positive. Scale bar 5 µm. Image of WT neuronwas modified from previous publication [6].

Additional file 3. Power spectrum of epileptic WT and Trpm4−/− mice is not different.Power spectral density plot of epileptic WTand Trpm4−/− mice during exploration.Statistics showing theta, alpha, betaand gammapower in epileptic WTand Trpm4−/−mice. n = 6 for WT and 6 for Trpm4−/− mice.

Additional file 4. Individual data points.

Additional file 5. Summary of statistics.

Acknowledgements
The research was performed in collaboration with the Nano-Bio-Imaging and the Histology and Light Microscopy core facility at the Szentágothai Research Centre of the University of Pécs. We thank V. Jasper for excellent technical assistance. This research work was conducted with the support of the National Academy of Scientist Education Program of the National Biomedical Foundation under the sponsorship of the Hungarian Ministry of Culture and Innovation (FEIF/646-4/2021- ITM_SZERZ).

Authors' contributions
MK performed the electrophysiological investigations. MK and LM accomplished the EEG and IHKA experiments. AK and NH-M performed the ISH and the immunostaining. MK prepared the figures and wrote the manuscript. RV provided the *Trpm4*$^{-/-}$ mice. PB, PK, and RV gave advice on the preparation of the manuscript. All authors have read and approved the final version of the manuscript.

Funding
Open access funding provided by University of Pécs. A.K was supported by the János Bolyai Research Scholarship of the Hungarian Academy of Sciences and the Research grant of Medical School, University of Pécs (KA-2021-23). M.K. was supported by the National Research Development and Innovation Office of Hungary (grant number: FK 135284). P.B. and P.K. were supported by the Health Subprogramme of the Thematic Excellence Programme (TKP2021-EGA-16) from the National Research Development and Innovation Office of Hungary. The authors declare no competing interest.

Availability of data and materials
All data generated or analyzed during this study are included in this published article and its supplementary information files. Individual data values for each figure can be found in Additional file 4. Summary of statistical analysis can be found in Additional file 5. Raw electrophysiological data, confocal images, and video files are available from M.K. upon reasonable request.

Declarations

Ethics approval and consent to participate
The experiments were reviewed and approved by Animal Welfare Committee at University of Pécs, National Scientific Ethical Committee on Animal Experimentation in Hungary (BA02/2000-10/2020 and BA02/2000-56/2022).

Consent for publication
Not applicable.

Competing interests
The authors declare that they have no competing interests.

Received: 22 November 2022 Accepted: 18 April 2023
Published online: 26 April 2023

References

1. Chang BS, Lowenstein DH. Epilepsy. N Engl J Med. 2003;349(13):1257–66.
2. Kwan P, Sander JW. The natural history of epilepsy: an epidemiological view. J Neurol Neurosurg Psychiatry. 2004;75(10):1376–81.
3. Scharfman HE. The enigmatic mossy cell of the dentate gyrus. Nat Rev Neurosci. 2016;17(9):562–75.
4. Scharfman HE. Electrophysiological evidence that dentate hilar mossy cells are excitatory and innervate both granule cells and interneurons. J Neurophysiol. 1995;74(1):179–94.
5. Scharfman HE, Myers CE. Hilar mossy cells of the dentate gyrus: a historical perspective. Front Neural Circuits. 2012;6:106.
6. Kecskés A, Czéh B, Kecskés M. Mossy cells of the dentate gyrus: drivers or inhibitors of epileptic seizures? Biochim Biophys Acta Mol Cell Res. 2022;1869(9):119279.
7. Bernard C, Esclapez M, Hirsch JC, Ben-Ari Y. Interneurones are not so dormant in temporal lobe epilepsy: a critical reappraisal of the dormant basket cell hypothesis. Epilepsy Res. 1998;32(1–2):93–103.
8. Bui AD, Nguyen TM, Limouse C, Kim HK, Szabo GG, Felong S, et al. Dentate gyrus mossy cells control spontaneous convulsive seizures and spatial memory. Science. 2018;359(6377):787–90.
9. Botterill JJ, Lu Y-L, LaFrancois JJ, Bernstein HL, Alcantara-Gonzalez D, Jain S, et al. An excitatory and epileptogenic effect of dentate gyrus mossy cells in a mouse model of epilepsy. Cell Rep. 2019;29(9):2875-2889.e6.
10. Blümcke I, Suter B, Behle K, Kuhn R, Schramm J, Elger CE, et al. Loss of hilar mossy cells in Ammon's horn sclerosis. Epilepsia. 2000;41(Suppl 6):S174–80.
11. Sloviter RS. Calcium-binding protein (calbindin-D28k) and parvalbumin immunocytochemistry: localization in the rat hippocampus with specific reference to the selective vulnerability of hippocampal neurons to seizure activity. J Comp Neurol. 1989;280(2):183–96.
12. Scharfman HE, Schwartzkroin PA. Electrophysiology of morphologically identified mossy cells of the dentate hilus recorded in guinea pig hippocampal slices. J Neurosci. 1988;8(10):3812–21.
13. Mathar I, Kecskes M, Van der Mieren G, Jacobs G, Camacho Londoño JE, Uhl S, et al. Increased β-adrenergic inotropy in ventricular myocardium from Trpm4-/- mice. Circ Res. 2014;114(2):283–94.
14. Simard C, Hof T, Keddache Z, Launay P, Guinamard R. The TRPM4 nonselective cation channel contributes to the mammalian atrial action potential. J Mol Cell Cardiol. 2013;59:11–9.
15. Mathar I, Jacobs G, Kecskes M, Menigoz A, Philippaert K, Vennekens R. TRPM4. Handb Exp Pharmacol. 2014;222:461–87.
16. Del Negro CA, Koshiya N, Butera RJJ, Smith JC. Persistent sodium current, membrane properties and bursting behavior of pre-bötzinger complex inspiratory neurons in vitro. J Neurophysiol. 2002;88(5):2242–50.
17. Picardo MCD, Sugimura YK, Dorst KE, Kallurkar PS, Akins VT, Ma X, et al. Trpm4 ion channels in pre-Bötzinger complex interneurons are essential for breathing motor pattern but not rhythm. PLoS Biol. 2019;17(2):e2006094.
18. Schattling B, Steinbach K, Thies E, Kruse M, Menigoz A, Ufer F, et al. TRPM4 cation channel mediates axonal and neuronal degeneration in experimental autoimmune encephalomyelitis and multiple sclerosis. Nat Med. 2012;18(12):1805–11.
19. Fearey BC, Binkle L, Mensching D, Schulze C, Lohr C, Friese MA, et al. A glibenclamide-sensitive TRPM4-mediated component of CA1 excitatory postsynaptic potentials appears in experimental autoimmune encephalomyelitis. Sci Rep. 2022;12(1):6000.
20. Viney TJ, Salib M, Joshi A, Unal G, Berry N, Somogyi P. Shared rhythmic subcortical GABAergic input to the entorhinal cortex and presubiculum. Elife. 2018;7:e34395.
21. Huang Y, Zhang L, Song N-N, Hu Z-L, Chen J-Y, Ding Y-Q. Distribution of Satb1 in the central nervous system of adult mice. Neurosci Res. 2011;71(1):12–21.
22. Danielson NB, Turi GF, Ladow M, Chavlis S, Petrantonakis PC, Poirazi P, et al. In vivo imaging of dentate gyrus mossy cells in behaving mice. Neuron. 2017;93(3):552-559.e4.
23. Veress R, Baranyai D, Hegyi B, Kistamás K, Dienes C, Magyar J, et al. Transient receptor potential melastatin 4 channel inhibitor 9-phenanthrol inhibits K(+) but not Ca(2+) currents in canine ventricular myocytes. Can J Physiol Pharmacol. 2018;96(10):1022–9.
24. Burris SK, Wang Q, Bulley S, Neeb ZP, Jaggar JH. 9-Phenanthrol inhibits recombinant and arterial myocyte TMEM16A channels. Br J Pharmacol. 2015;172(10):2459–68.
25. Bean BP. The action potential in mammalian central neurons. Nat Rev Neurosci. 2007;8(6):451–65.

26. Lévesque M, Avoli M. The kainic acid model of temporal lobe epilepsy. Neurosci Biobehav Rev. 2013;37(10 Pt 2):2887–99.
27. Huneau C, Benquet P, Dieuset G, Biraben A, Martin B, Wendling F. Shape features of epileptic spikes are a marker of epileptogenesis in mice. Epilepsia. 2013;54(12):2219–27.
28. Umpierre AD, Bennett IV, Nebeker LD, Newell TG, Tian BB, Thomson KE, et al. Repeated low-dose kainate administration in C57BL/6J mice produces temporal lobe epilepsy pathology but infrequent spontaneous seizures. Exp Neurol. 2016;279:116–26.
29. Lin H, Holmes GL, Kubie JL, Muller RU. Recurrent seizures induce a reversible impairment in a spatial hidden goal task. Hippocampus. 2009;19(9):817–27.
30. Menigoz A, Ahmed T, Sabanov V, Philippaert K, Pinto S, Kerselaers S, et al. TRPM4-dependent post-synaptic depolarization is essential for the induction of NMDA receptor-dependent LTP in CA1 hippocampal neurons. Pflugers Arch. 2016;468(4):593–607.
31. Bovet-Carmona M, Menigoz A, Pinto S, Tambuyzer T, Krautwald K, Voets T, et al. Disentangling the role of TRPM4 in hippocampus-dependent plasticity and learning: an electrophysiological, behavioral and FMRI approach. Brain Struct Funct. 2018;223(8):3557–76.
32. Riquelme D, Peralta FA, Navarro FD, Moreno C, Leiva-Salcedo E. I(CAN) (TRPM4) contributes to the intrinsic excitability of prefrontal cortex layer 2/3 pyramidal neurons. Int J Mol Sci. 2021;22(10):5268.
33. Mironov SL. Metabotropic glutamate receptors activate dendritic calcium waves and TRPM channels which drive rhythmic respiratory patterns in mice. J Physiol. 2008;586(9):2277–91.
34. Li K, Abbott SBG, Shi Y, Eggan P, Gonye EC, Bayliss DA. TRPM4 mediates a subthreshold membrane potential oscillation in respiratory chemoreceptor neurons that drives pacemaker firing and breathing. Cell Rep. 2021;34(5):108714.
35. Li K, Shi Y, Gonye EC, Bayliss DA. TRPM4 contributes to subthreshold membrane potential oscillations in multiple mouse pacemaker neurons. eNeuro. 2021;8(6):ENEURO.0212-21.2021.
36. Voss LJ, Sleigh JW, Barnard JPM, Kirsch HE. The howling cortex: seizures and general anesthetic drugs. Anesth Analg. 2008;107(5):1689–703.
37. Löscher W, Hirsch LJ, Schmidt D. The enigma of the latent period in the development of symptomatic acquired epilepsy - traditional view versus new concepts. Epilepsy Behav. 2015;52(Pt A):78–92.
38. Senzai Y, Buzsáki G. Physiological properties and behavioral correlates of hippocampal granule cells and mossy cells. Neuron. 2017;93(3):691-704.e5.
39. Vandewiele F, Pironet A, Jacobs G, Kecskés M, Wegener J, Kerselaers S, et al. TRPM4 inhibition by meclofenamate suppresses Ca2+-dependent triggered arrhythmias. Eur Heart J. 2022;43(40):4195–207.
40. Lehnart SE, Mongillo M, Bellinger A, Lindegger N, Chen B-X, Hsueh W, et al. Leaky Ca2+ release channel/ryanodine receptor 2 causes seizures and sudden cardiac death in mice. J Clin Invest. 2008;118(6):2230–45.
41. Tadel F, Baillet S, Mosher JC, Pantazis D, Leahy RM. Brainstorm: a user-friendly application for MEG/EEG analysis. Comput Intell Neurosci. 2011;2011:879716.
42. Kecskés A, Pohóczky K, Kecskés M, Varga ZV, Kormos V, Szőke É, et al. Characterization of neurons expressing the novel analgesic drug target somatostatin receptor 4 in mouse and human brains. Int J Mol Sci. 2020;21(20):7788.

Publisher's Note